Chinese Chemical Letters 32 (2021) 2648–2658

Contents lists available at ScienceDirect

Chinese Chemical Letters

journal homepage: www.elsevier.com/locate/cclet

Review

# Role of MXene surface terminations in electrochemical energy storage: A review

Zhuoheng Bao, Chengjie Lu, Xin Cao, Peigen Zhang, Li Yang, Heng Zhang, Dawei Sha, Wei He, Wei Zhang, Long Pan*, Zhengming Sun*

*School of Materials Science and Engineering, Southeast University, Nanjing 211189, China*

ARTICLE INFO

*Article history:*
Received 20 December 2020
Received in revised form 18 January 2021
Accepted 6 February 2021
Available online 9 February 2021

*Keywords:*
MXene
Surface terminations
Energy storage
First-principles calculation
Batteries
Supercapacitors

ABSTRACT

MXenes are a group of recently discovered 2D materials and have attracted extensive attention since their first report in 2011; they have shown excellent prospects for energy storage applications owing to their unique layered microstructure and tunable electrical properties. One major feature of MXenes is their tailorable surface terminations (*e.g.*, −F, −O, −OH). Numerous studies have indicated that the composition of the surface terminations can significantly impact the electrochemical properties of MXenes. Nonetheless, the underlying mechanisms are still poorly understood, mainly because of the difficulties in quantitative analysis and characterization. This review summarizes the latest research progress on MXene terminations. First, a systematic introduction to the approaches for preparing MXenes is presented, which generally dominates the surface terminations. Then, theoretical and experimental efforts regarding the surface terminations are discussed, and the influence of surface terminations on the electronic and electrochemical properties of MXenes are generalized. Finally, we present the significance and research prospects of MXene terminations. We expect this review to encourage research on MXenes and provide guidance for usingthese materials for batteries and supercapacitors.



## 1. Introduction

There is great demand for renewable energy storage techniques because they are essential for ensuring the sustainable development of our society. Rechargeable batteries and supercapacitors are the most widely investigated and commercialized energy storage systems that require advanced materials to deliver high energy and power densities.

Two-dimensional (2D) materials are promising candidates in the energy storage field owing to their unique physical and electronic properties, high specific surface area, and variable active sites [1–4]. Since the discovery of graphene [5], 2D materials have been of particular interest. In the past few years, several 2D materials have been developed, such as hexagonal boron nitride (h-BN) [6], transition metal dichalcogenides (TMDs) [7], silicone [8], germanane [9] and phosphorene [10].

Recently, a group of transition metal carbides or nitrides, with the general formula $M_{n+1}X_nT_x$, has become one of the latest members in the 2D materials family [11], where M is an early transition metal element, X is carbon and/or nitrogen, and T represents surface terminations ($n$ = 1–4). Because they are generally synthesized from MAX precursors by selectively removing the lattice A atoms using proper etchants, the name "MXene," similar to graphene, is given [12]. The chemical composition of the MAX precursors and the atomic structure of MXenes are shown in Fig. 1.

The discovery of MXenes dates back to 2011, when Naguib *et al.* [11] first reported the $Ti_3C_2T_x$ MXene by removing the Al atoms from $Ti_3AlC_2$ using a HF solution. Since then, various techniques have been developed to synthesize MXenes. To date, more than 30 members have been successfully obtained in experiments. It is worth noting that the classification of these MXenes only considers the types and contents of M and X, while the composition of terminations is ignored. The terminations are due to inevitable and complex reaction processes during preparation. The complexity of terminations, including their random arrangement, variable composition, and unique bonding features, hinders the accurate characterization of MXenes. Taking $Ti_3C_2T_x$ as an example, Mashtalir *et al.* [13] reported a chemical formula of $Ti_{2.94}C_2F_2O_{0.55}(OH)_{0.65}$ by HF etching, indicating the diverse composition

* Corresponding authors.
*E-mail addresses:* panlong@seu.edu.cn (L. Pan), zmsun@seu.edu.cn (Z. Sun).

https://doi.org/10.1016/j.cclet.2021.02.012

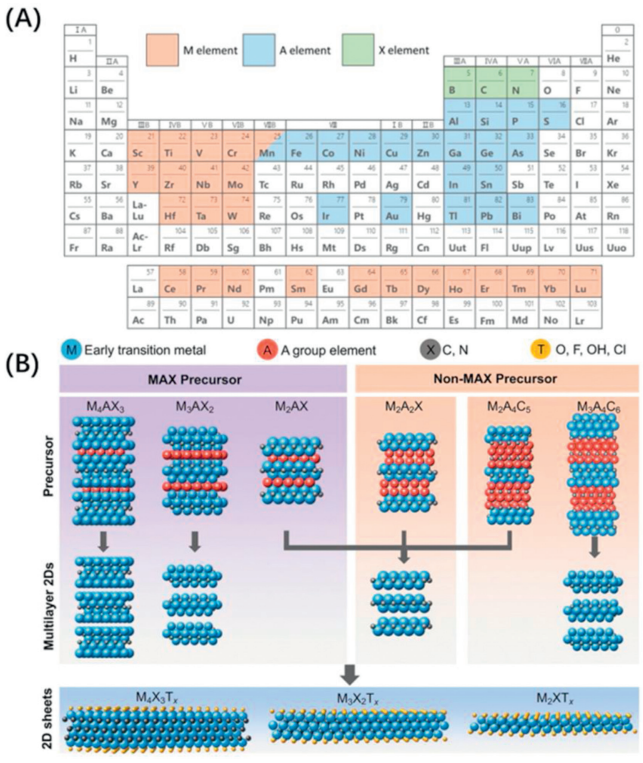


**Fig. 1.** (A) Periodic table with candidate elements in MAX phases. (B) Synthesis and structures of three major types of MXene systems, namely $M_2XT_x$, $M_3X_2T_x$ and $M_4X_3T_x$. Reproduced with permission [12]. Copyright 2019, Springer Nature.

and non-stoichiometry of terminations. However, a different chemical formula of $Ti_3C_2(OH)_{0.12}F_{0.8}O_{0.54}$ was reported by Hope *et al.* [14] using the same etching strategy.

For the convenience of theoretical research, simplified models that contain single terminations, such as $Ti_3C_2F_2$, $Ti_3C_2O_2$ and $Ti_3C_2(OH)_2$, are usually proposed, assuming that the terminations are uniformly distributed over the surface [15,16]. These studies revealed that the physical properties of MXenes, such as the band gap [17], electronic mobility [18], metallicity [19] and magnetism [20], are markedly associated with the terminations. Moreover, the electrochemical performance of MXenes can be tailored by manipulating the surface terminations. For instance, −F terminations are believed to hamper the capacity of MXenes in ion batteries [17]. With a proper synthesis strategy, the capacity of MXenes can be remarkably improved by increasing the ratio of −O:−F terminations [21].

In this review, the latest progress in the study of MXene terminations for energy storage applications is summarized. The feasible etching strategies for the synthesis of MXenes are generalized first, which dominates the composition of the surface terminations. Subsequently, simulation results of first-principles calculations are summarized, illustrating the role of surface terminations in the energy storage process. Finally, strategies for manipulating the surface terminations are discussed, and the factors contributing to the enhanced performance of MXene electrodes are discussed. At the end of this review, the present status and future challenges of MXene termination design are presented.

## 2. Origin of terminations: synthesis strategies

The crystallographic structure of MAX phases can be described as the stacking of transition metal carbide/nitride [$M_6X$] octahedrons interleaved with a plane of pure A atoms. This layered feature endows the A atoms in the lattice with high mobility along the basal plane. By utilizing proper etching methods, the A layers can be removed from MAX crystal structures. The resulting exposed M-site atoms exhibit high reducibility, thus making MXenes reactive to the etchants and solvent. When reactions occur and M atoms lose electrons, the negatively charged groups in the environment form bonds with the exposed M atoms to ensure conservation of charge, which introduces terminations.

To date, several etchants have been used efficiently for the synthesis of MXenes. The products vary with the etching parameters, mainly in the composition of surface terminations and the microstructure of nanoflakes, including the interlayer spacing and surface area.

**Table 1**
Experiment parameters for the synthesis of MXenes by HF etching.

| Structure | MAX precursor | Etching parameter [a] | Obtained MXene [ref.] |
|---|---|---|---|
| $M_{4/3}XT_x$ | $(Mo_{2/3}Y_{1/3})_2AlC$ | 10 wt% + 72 h | $Mo_{4/3}CT_x$ [22] |
| | $(Nb_{2/3}Sc_{1/3})_2AlC$ | 48 wt% + 12 h | $Nb_{4/3}CT_x$ [23] |
| | $(W_{2/3}Sc_{1/3})_2AlC$ | 48 wt% + 30 h | $W_{4/3}CT_x$ [24] |
| | $(W_{2/3}Y_{1/3})_2AlC$ | 48 wt% + 30 h | $W_{4/3}CT_x$ [24] |
| $M_2XT_x$ | $Ti_2AlC$ | 10 wt% + 10 h | $Ti_2CT_x$ [25] |
| | $V_2AlC$ | 50 wt% + 90 h | $V_2CT_x$ [26] |
| | $Nb_2AlC$ | 50 wt% + 90 h | $Nb_2CT_x$ [26] |
| | $(Mo_{2/3}Y_{1/3})_2AlC$ | 48 wt% + 10 h | $(Mo_{2/3}Y_{1/3})_2CT_x$ [22] |
| | $(Ti_{1/2}Nb_{1/2})_2AlC$ | 50 wt.% + 28 h | $(Ti_{1/2}Nb_{1/2})_2CT_x$ [25] |
| | $Mo_2Ga_2C$ | 50 wt% + 160 h (55 °C) | $Mo_2CT_x$ [27] |
| $M_3X_2T_x$ | $Ti_3AlC_2$ | 50 wt% + 2 h | $Ti_3C_2T_x$ [25] |
| | $Ti_3AlCN$ | 30 wt% + 18 h | $Ti_3CNT_x$ [25] |
| | $(Cr_{1/2}V_{1/2})_3AlC_2$ | 50 wt.% + 69 h | $(Cr_{1/2}V_{1/2})_3C_2T_x$ [25] |
| | $(Mo_{2/3}Ti_{1/3})_3AlC_2$ | 48 wt% + 48 h | $(Mo_{2/3}Ti_{1/3})_3C_2T_x$ [28] |
| | $(Mo_{2/3}Sc_{1/3})_3AlC_2$ | 48 wt% + 16 h (50 °C) | $(Mo_{2/3}Sc_{1/3})_3C_2T_x$ [29] |
| | $Zr_3Al_3C_5$ [b] | 50 wt% + 72 h | $Zr_3C_2T_x$ [30] |
| | $Hf_3[Al(Si)]_4C_6$ [b] | 35 wt% + 60 h | $Hf_3C_2T_x$ [31] |
| $M_4X_3T_x$ | $V_4AlC_3$ | 40 wt% + 165 h | $V_4C_3T_x$ [32] |
| | $Nb_4AlC_3$ | 48 wt% + 96 h | $Nb_4C_3T_x$ [33] |
| | $Ta_4AlC_3$ | 50 wt% + 72 h | $Ta_4C_3T_x$ [25] |
| | $(Nb_{4/5}Ti_{1/5})_4AlC_3$ | 50 wt% + 96 h | $(Nb_{4/5}Ti_{1/5})_4C_3T_x$ [34] |
| | $(Mo_{1/2}Ti_{1/2})_4AlC_3$ | 48 wt% + 90 h (50 °C) | $(Mo_{1/2}Ti_{1/2})_4C_3T_x$ [28] |

[a] The reaction temperature is room temperature unless otherwise stated.
[b] Non-MAX phase precursors.

### 2.1. Hydrofluoric acid-based etching

Hydrofluoric acid (HF) was the first etchant used to fabricate MXenes and has been widely adopted in their synthesis. It possesses the advantages of a simple process, low cost, and high yield. To date, more than 20 members of the MXene family have been successfully obtained using this method. The corresponding reaction mechanism is described by Eq. 1. Simultaneously, the introduction of surface terminations is generally inevitable in solutions, according to Eqs. 2 and 3 [11].

$$M_{n+1}AlX_n + 3HF = AlF_3 + M_{n+1}X_n + 3/2H_2 \quad (1)$$

$$M_{n+1}X_n + 2H_2O = M_{n+1}X_n(OH)_2 + H_2 \quad (2)$$

$$M_{n+1}X_n + 2HF = M_{n+1}X_nF_2 + H_2 \quad (3)$$

A large variety of MXenes were successfully synthesized by HF etching [22–34]. Etching parameters, including the HF concentration, treatment time, and temperature, are of particular significance to the purity and composition of MXenes. The present results available in the literature are listed in Table 1. It can be seen that Al-based MAX phases are mostly adopted as precursors because Al possesses a relatively low reduction potential [35]. Moreover, some non-MAX compounds with similar structures and Al atoms, such as $Zr_3Al_3C_5$ [30] and $Hf_3[Al(Si)]_4C_6$ [31], can also transform into corresponding MXenes when properly etched with a HF solution. For non-Al-based MAX phases, a pure HF solution cannot etch the A layers because of their strong binding energy to M atoms. However, the addition of strong oxidants significantly improves the etching efficiency. In 2018, Alhabeb *et al.* [36] developed a composite solution to remove Si atoms from $Ti_3SiC_2$ using a mixture of HF and strong oxidants, including hydrogen peroxide and ammonium persulfate.

It is worth noting that the chemical reactivity of M-site atoms can also be reflected in the etching process. Persson *et al.* [22] proposed that $(Mo_{2/3}Y_{1/3})_2AlC$, an i-MAX phase with Mo and Y atoms arranged orderly on the M layer, could also be applied as a precursor. The composition of the product varies with the etching parameters: $(Mo_{2/3}Y_{1/3})_2CT_x$ is obtained with the removal of Al atoms at the A-site using a high-concentration HF solution (48% + 10 h), while $Mo_{4/3}CT_x$ is achieved with the removal of Y and Al atoms from M- and A-sites using a low-concentration HF solution (10% + 72 h).

MXenes etched using a HF solution have composite terminations (including –F, –O and –OH) that largely depend on the reaction environment. Unfortunately, earlier studies have failed to focus on the composition of terminations. Recently, Gentile *et al.* [37] found that high-concentration HF solutions may result in accordion-like MXenes with a predominant amount of –F terminations. In contrast, MXenes under milder etching conditions have larger amounts of –OH terminations. In the presence of these hydrophilic terminations, intercalating agents, such as dimethyl sulfoxide (DMSO), dimethylformamide (DMF), hydrazine hydrate (HM), cetyltrimethylammonium bromide (CTAB) and tetrabutylammonium hydroxide (TBAOH), can form hydrogen bonds with –F, –O and –OH terminations. The intercalation of macromolecules strongly promotes interlayer expansion and prevents self-restacking of MXenes [38].

In 2014, Ghidiu *et al.* [39] formed a HF etchant *in situ* using a mixture of LiF and HCl, which is abbreviated as LiF/HCl below, as shown in Fig. 2A. The intercalation of hydrated cations is proposed to be the major factor contributing to the large interlayer spacing, which makes $Ti_3C_2T_x$ easy to exfoliate without the use of extra intercalation agents. Lipatov *et al.* [40] optimized this etching strategy by increasing the amount of LiF. The purity of the prepared $Ti_3C_2T_x$ MXene was improved, which could be simply exfoliated by handshaking because of the increased proportion of pre-intercalated cations. Following the principle of forming a HF etchant *in*

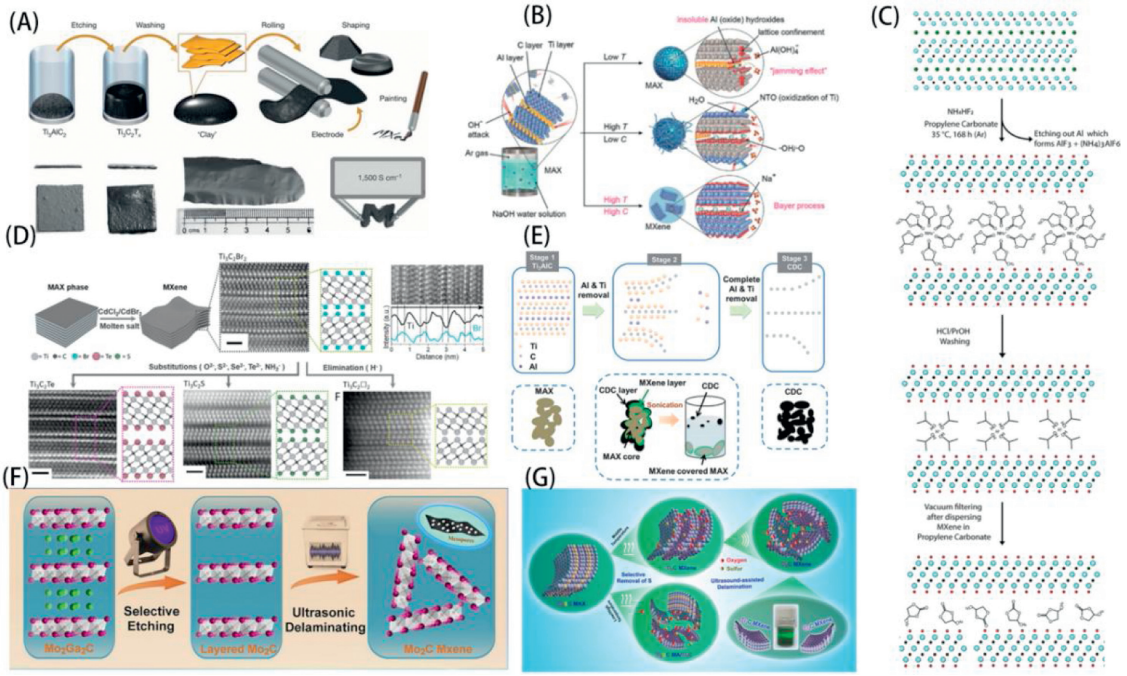


**Fig. 2.** Various MXene synthesis methods. (A) LiF/HCl-etched "clay-like" MXenes. Reproduced with permission [39]. Copyright 2014, Springer Nature. (B) Alkali-etched MXenes. Reproduced with permission [60]. Copyright 2018, Wiley. (C) $NH_4HF_2$-etched MXenes. Reproduced with permission [54]. Copyright 2020, Elsevier. (D) Molten-salt-etched MXenes. Reproduced with permission [58]. Copyright 2020, Science. (E) Electrochemically etched MXenes. Reproduced with permission [61]. Copyright 2013, Royal Society of Chemistry. (F) UV-induced selective-etched MXenes. Reproduced with permission [64]. Copyright 2020, Elsevier. (G) MXenes fabricated by thermal reduction. Reproduced with permission [65]. Copyright 2020, Elsevier.

*situ*, other combinations of fluorine salts (*e.g.*, NaF, KF and $NH_4F$) and acids (*e.g.*, $H_2SO_4$) have also been shown to be feasible for the synthesis of MXenes [41] with tailorable interlayer spacings, termination species, and residual cations. Not surprisingly, –Cl terminations are introduced by LiF/HCl etching, leading to a decrease in the proportion of –F terminations. According to Kajiyama *et al.* [42], the F in $Ti_3C_2T_x$ etched using a LiF/HCl solution accounted for 6.7 at% of the product, which was much smaller than that obtained using a HF etchant (33.3 at% F), as reported by Li *et al.* [43]. LiF/HCl solution etchants have been widely applied, and various MXenes have been successfully obtained, including $Mo_2CT_x$ [27], $W_{4/3}CT_x$ [24], $(Cr_{2/3}Ti_{1/3})_3C_2T_x$ [28], $(Nb_{4/5}Zr_{1/5})_4C_3T_x$ [34], $Ti_2CT_x$ [44], $V_2CT_x$ [45], $TiVCT_x$ [46] and $V_2NT_x$ [47]. Furthermore, LiF/HCl etching can simplify the exfoliation process. Through this method, numerous few-layered-MXene-based derivatives and composite materials have been successfully synthesized by subsequent reactions and widely applied in batteries [48], supercapacitors [49], catalysts [50] and sensors [51].

Apart from HF and LiF/HCl, $NH_4HF_2$ is another feasible fluorine-containing salt for the synthesis of MXenes, which has attracted particular interest owing to its potential application in organic solvents. Halim *et al.* [52] first managed to remove Al atoms from $Ti_3AlC_2$ films at room temperature using an $NH_4HF_2$ solution. Thereafter, Feng *et al.* [53] found that $NH_4HF_2$-etched $Ti_3C_2T_x$ possessed better thermal stability and oxidation resistance than those of HF-etched ones due to a proper combination of surface terminations. Recently, Natu *et al.* [54] successfully applied $NH_4HF_2$ salt to synthesize the $Ti_3C_2T_x$ MXene in organic polar solvents, the scheme of which is illustrated in Fig. 2C. Moreover, the obtained flakes were characterized to be mainly covered by –F, accounting for more than 70% of the total surface terminations, which is the highest proportion in the reported MXenes to date.

In conclusion, solution etching yields high-purity products because of the good reaction environment and homogenous dispersion. In addition, fluoride salt/acid etching methods allow solvent and solute to be inserted between the MXene layers, resulting in a large interlayer spacing with three or more termination species on the surface. However, it remains challenging to experimentally determine the role of surface terminations since quantitative control techniques to regulate surface terminations are still lacking.

### 2.2. Molten salt etching

The complex solution environment in the fluorine solution etching process makes it generally impossible to obtain MXenes with a single type of termination. Researchers have constantly sought a simple etching method that avoids aqueous solutions. Molten salts are promising reactants because they are corrosive and can provide a simple reaction environment.

In 2016, Urbankowski *et al.* [55] synthesized $Ti_4N_3T_x$ from its precursor $Ti_4AlN_3$ using a molten fluorine salt (a mixture of LiF, NaF and KF) for the first time. With the assistance of organic molecule intercalation and ultrasound treatment, exfoliated $Ti_4N_3T_x$ flakes were successfully obtained. This was the first reported attempt to synthesize MXenes using a water-free method. However, the presence of a variety of impurities, including $K_3AlF_6$ and $Na_3AlF_6$, hampered its widespread use. Furthermore, mixed –F, –O and –OH terminations were still detected in the delaminated $Ti_4N_3T_x$.

In 2019, Li *et al.* [56] demonstrated a general approach to fabricate Zn-based MAX phases, in which the original A-site atoms were replaced by Zn from the molten $ZnCl_2$ salt, following Eq. 5. Subsequently, the lattice Zn atoms were removed owing to the strong Lewis acid effect, according to Eq. 6, forming –Cl-terminated MXenes (Cl-MXene). Using this molten salt etching method, $Ti_3AlC_2$ and $Ti_2AlC$ MAX phases were successfully transformed into $Ti_3C_2Cl_2$ and $Ti_2CCl_2$ MXenes. Thereafter, a systematic study using other Lewis acid molten salts, including $CuCl_2$, $NiCl_2$, AgCl and $FeCl_2$, was conducted by the same research group [57]. The results suggest that the redox potential is the key factor that determines the feasibility of the replacement reaction shown in Eq. 5. In other words, other A-site elements in MAX phases could also be removed using this molten salt etching method by choosing proper Lewis acid molten salts.

$$Ti_3AlC_2 + 1.5ZnCl_2 = Ti_3ZnC_2 + 0.5Zn + AlCl_3(g) \quad (5)$$

$$Ti_3ZnC_2 + ZnCl_2 = Ti_3C_2Cl_2 + 2Zn \quad (6)$$

Characterization of the MXenes suggested that the surface termination was generally pure –Cl. The absence of –O and –OH implies that the molten salts effectively prevented oxidation and hydroxylation of MXenes. Moreover, the –Cl termination was less strongly bonded to the M atoms than the –F, –OH and –O terminations, which opened possibilities for the surface manipulation of Cl-MXenes. Kamysbayer *et al.* [58] successfully synthesized –Cl- and –Br-terminated MXenes using $CdCl_2$ and $CdBr_2$ molten salts, respectively, as shown in Fig. 2D. The obtained MXenes were mixed with molten alkali salts, and the termination substitution reactions were detected. Subsequently, various types of MXenes, such as $Ti_3C_2Se$, $Ti_3C_2S$ and $Ti_3C_2NH$, were formed. This work indicated the possibility of tailoring the chemical composition of the surface terminations through the displacement reaction of molten salt as well as a new strategy for introducing novel terminations to MXenes.

### 2.3. Other synthesis methods

In addition to molten salts, researchers have been seeking other fluorine-free etching methods. In 2017, Li *et al.* [59] first reported the removal of lattice Al atoms from $Ti_3AlC_2$ using a highly concentrated KOH solution at 180 °C, which occurred as follows:

$$Ti_3AlC_2 + KOH + H_2O = Ti_3C_2 + KAlO_2 + 3/2H_2 \quad (7)$$

$$Ti_3C_2 + 2H_2O = Ti_3C_2(OH)_2 + H_2 \quad (8)$$

In 2018, Li *et al.* [60] improved this alkali-based etching method by increasing the processing temperature up to 270 °C using a 27.5 mol/L NaOH solution, as shown in Fig. 2B. The obtained $Ti_3C_2T_x$ MXene was mainly terminated with –OH and –O. Compared with acid etching methods, the alkali-based etchants create a fluorine-free environment. However, the high processing temperature and pressure inevitably cause oxidation of the MXenes.

Electrochemically assisted etching is another feasible method for preparing MXenes. Initially, Sun *et al.* [61] studied the electrochemical corrosion behavior of porous $Ti_2AlC$ as an electrode in an HCl solution. The prepared electrodes are shown in Fig. 2E. After more than 5 d of electrification, $Ti_2AlC$ was slowly converted to $Ti_2CT_x$, which was mainly covered by –Cl and –O terminations. However, a dense carbon layer formed on the surface of $Ti_2AlC$ with the loss of Ti atoms due to the over-etching of MAX phases. The unexpected carbon layer resulted in a limited etching degree. Yang *et al.* [62] successfully synthesized $Ti_3C_2T_x$ from $Ti_3AlC_2$ by electrochemically assisted etching using an $NH_4Cl$ solution. Tetramethylammonium hydroxide (TMAOH) was added to the solution as an intercalation agent to avoid the formation of a dense carbon layer, which allowed etching and exfoliation to be performed simultaneously. In 2019, Pang *et al.* [63] prepared a $Ti_2AlC$-based composite electrode for electrochemical etching

using HCl as the electrolyte. The $Ti_2CT_x$ nanosheets were successfully fabricate after etching at 50 °C for 9 h. Subsequently, $V_2CT_x$ and $Cr_2CT_x$ were prepared using a similar process.

The types of terminations introduced by the different strategies are listed in Table 2. In addition, the advantages and disadvantages of each strategy are summarized. Recently, a variety of new MXene preparation methods have emerged, such as ultraviolet (UV)-assisted etching [64] and thermal reduction [65], which are shown in Figs. 2F and G. However, these novel fluorine-free etching methods are only applicable for the synthesis of a few specific MXenes, and the composition of the terminations are poorly analyzed. Therefore, further studies must be conducted in the future to examine the practicability of the above etching methods.

## 3. Influence of terminations: Electronic and electrochemical properties

Owing to the complexity of terminations with diverse species and variable compositions, it is difficult to control terminations accurately or to reveal their influence. Alternatively, first-principles calculations serve as a reliable method to quickly understand the structure and performance impacts of terminations. First-principles calculations have been performed to study the physical and chemical behaviors of MXenes, including mechanical [66], electronic [67–69], magnetic [69], optical [16] and thermoelectric [70] properties. The determination of bonding features between terminations and surface transition metals is determined prior to the simulation of MXene structures. Taking $M_2XT_2$ as an example, there are three possible sites on the surface to bridge the terminations, as shown in Fig. 3A. Model 1: two terminations are located directly on top of two M atoms, which are marked as "M-top". Model 2: two terminations are located on the hollow position among three adjacent M atoms, directly facing the M atom in the lattice, which are marked as "M-hollow". Model 3: two terminations are located on the hollow position among three adjacent M atoms, directly facing the X atom in the lattice, which are marked as "X-hollow". Tang *et al.* [17] proposed that Model 2 should be the most stable configuration in most MXenes by computing the formation energies. However, the configuration of Model 3 has been reported in recent literature [71], in which an electron exchange effect between lattice carbon and surface terminations was determined to stabilize these materials.

The formation energy can be used to evaluate the thermal stability of terminated MXenes. First-principles calculations have shown that terminating with non-metal atoms yields a negative formation energy, indicating that the terminations are strongly bonded to the transition metals on the surface [69]. The formation energy varies with the type of element owing to the difference in bond energy between M and T atoms. In addition, the mechanical properties of MXenes can be affected by the formation energy. −O-terminated MXenes present smaller lattice parameters and larger elastic constants than those terminated by −F and −OH [66], as shown in Figs. 3B and C. It is notable that some other terminations, such as −N and −S, are also theoretically stable according to phonon frequency analyses, which encourages the potential modification of MXenes.

Although pristine MXenes are metallic and have high conductivity, terminations may alter MXenes into semimetals or semiconductors [19,72]. Zha *et al.* [66] calculated that $Sc_2CT_2$ (T = F, OH and O) had energy gaps of 1.03, 0.45 and 1.80 eV, respectively. Differences in band structures were also detected in $Ti_2CT_2$ and $V_2CT_2$, as shown in Figs. 3D and E. The electronic structures of MXenes are strongly dependent on the isolating difference in transition metals as well as the element species inthe terminations. The hybridization between the p orbitals of F or O atoms and the d orbitals of M atoms contributes to the formation of new bands below the Fermi level. In other words, terminations shift the Fermi energy to the center of the gap [71]. In addition, nearly free electron (NFE) states located outside the atomic structure were predicted for a variety of MXenes [73]. The NFE states of some −OH terminated MXenes, such as $Ti_2C(OH)_2$, $Zr_2C(OH)_2$ and $Zr_2N(OH)_2$, were partially occupied, which provided transmission channels for electron transport.

Furthermore, terminations also affect energy storage properties. First-principles calculations have been used to analyze the mechanisms and predict the energy storage properties of MXenes on the atomic scale. A variety of bare and terminated MXenes have been systematically studied, including $Ti_2CT_x$ [21,74], $V_2CT_x$ [75–77], $Mo_2CT_x$ [78], $Ti_2NT_x$ [79], $V_2NT_x$ [79], $Fe_2CT_x$ [80], $Ti_3C_2T_x$ [17,81], $V_3C_2T_x$ [81], $Nb_3C_2T_x$ [81], $Hf_3C_2T_x$ [81] and $Zr_3C_2T_x$ [81]. Numerous calculation results reveal that terminations interacting directly with ions have a significant influence on the ion adsorption and diffusion process, the models of which are shown in Fig. 4. The capacity also depends on the type of termination. For instance, the theoretical capacities of bare $Ti_3C_2$, $Ti_3C_2O_2$, $Ti_3C_2F_2$ and $Ti_3C_2(OH)_2$ in Li-ion batteries were 320, 268, 130 and 76 mAh/g, respectively [17,21,82]. Additional calculation proofs are presented in Fig. 5 [21].

The finding that non-halogen elements with large atomic radii were more conducive to energy storage inspired researchers to arrange various possible terminations, including −S and −N, on the surface of MXenes, thereby revealing the effect of these terminations. Studies have shown that −S-terminated MXenes are promising ion battery anode materials. Metha *et al.* [78] found that −S terminations in $Mo_2C$ could substantially increase the Li adsorption ability, which consequently improved the $Li^+$ storage capacity to 410 mAh/g. Yan *et al.* [77] found that $V_2CT_x$ (T = O and S) possessed low barriers (0.15 and 0.22 eV) for the diffusion of Li atoms, resulting in a high theoretical capacity (367.64 and 301.22 mAh/g). Meng *et al.* [83] proposed that a $Ti_3C_2S_2$ monolayer was capable of absorbing double-layered Na ions, contributing to a theoretical capacity of 463 mAh/g, which is even larger than that of bare-$Ti_3C_2$. −S-terminated $Ti_2C$ was simulated by Wang *et al.* [74] and exhibited good theoretical capacities of 935.57 mAh/g in Na-ion batteries and 1871.13 mAh/g in Mg-ion batteries. Lee *et al.* [80] predicted a new series of MXenes, $Fe_2CT_x$ (T = O and S). Although the capacity of $Fe_2CS_2$ (642 mAh/g) was lower than that of $Fe_2CO_2$

**Table 2**
Comparison of the advantages and disadvantages of various synthesis strategies.

| Strategies | Terminations | Advantages | Disadvantages |
|---|---|---|---|
| HF-based etching | −F, −OH, −O, −Cl | High efficiency<br>Universal | Toxic<br>Eco-unfriendly |
| Molten salt etching | −Cl, −Br or −I | Nearly single termination | High-temperature synthesis (> 600 °C) |
| Alkali-based etching | −OH, −O | Non-toxic | Low efficiency<br>High-temperature, high-pressure synthesis |
| Electrochemically assisted etching | −Cl, −O | Non-toxic | Low efficiency<br>Over-etching |

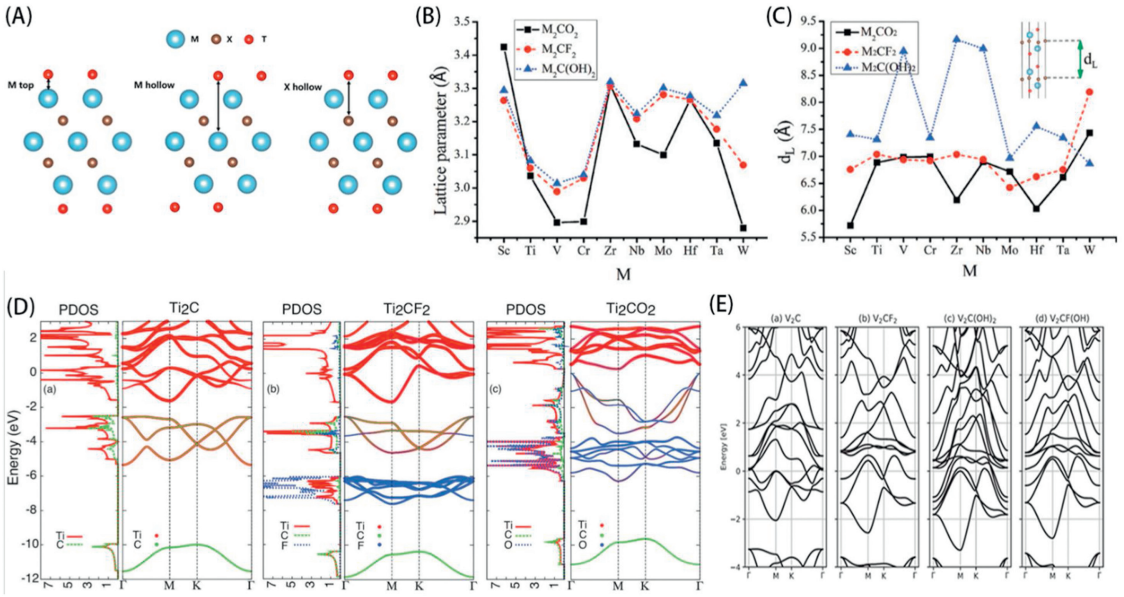


**Fig. 3.** (A) Possible models for $M_2XT_2$ systems. (B) Lattice parameters in the xy-plane for $M_2CT_2$ MXenes. Reproduced with permission [66]. Copyright 2015, IOP. (C) Layer thicknesses for $M_2CT_2$ MXenes, where the inset graph indicates the layer thickness. Reproduced with permission [66]. Copyright 2015, IOP. (D) Density of states and band structures of $Ti_2C$, $Ti_2CF_2$ and $Ti_2CO_2$. Reproduced with permission [71]. Copyright 2013, Royal Society of Chemistry. (E) Electronic band structures of $V_2C$, $V_2CF_2$, $V_2C(OH)_2$ and $V_2CF(OH)$, where the Fermi level is designated as zero energy. Reproduced with permission [68]. Copyright2018, American Physical Society.

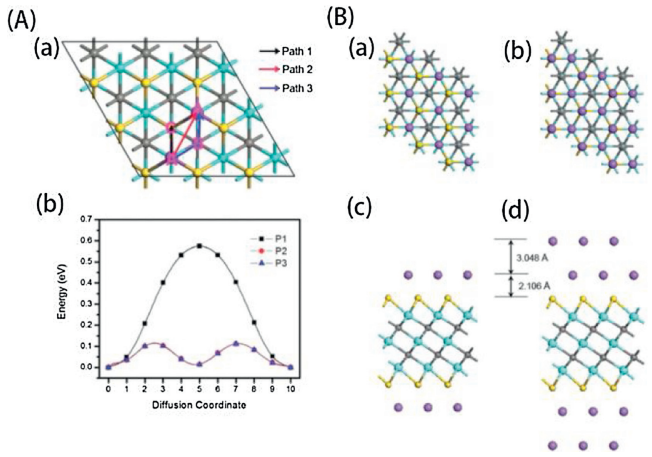


**Fig. 4.** Models for simulating electrochemical performances of MXenes, taking $Ti_3C_2S_2$ and Na atoms as an example. (A) Na diffusion on a $Ti_3C_2S_2$ monolayer: (a) three possible diffusion paths and (b) the corresponding diffusion energy. (B) Na adsorption on a $Ti_3C_2S_2$ monolayer: (a, c) single layer and (b, d) bilayer Na atoms. Reproduced with permission [83]. Copyright 2009, Royal Society of Chemistry.

(775 mAh/g), the $Al^{3+}$ diffusion barrier in $Fe_2CS_2$ (0.47 eV) was considerably lower than that in $Fe_2CO_2$ (0.71 eV), indicating enhanced Al-ion transport with O-to-S replacement. They proposed $Fe_2CS_2$ as a promising electrode for Al-ion batteries.

When applied to electrochemical capacitors, MXenes always exhibit capacitive or pseudocapacitive behavior [84]. These behaviors are highly dependent on the surface states of MXenes. Recent work has shown that pseudocapacitive behavior occurs because of the orbital coupling of adsorbed cation states with surface-terminated MXene states [85]. To understand the role of terminations, Wang *et al.* [86] calculated the theoretical pseudocapacitance limits of $Ti_3C_2T_x$ (T = bare, O and S). Assuming $H^+$ fully covered the surface, the pseudocapacitance of bare $Ti_3C_2$ (2018.8 F/g) was much higher than those of $Ti_3C_2O_2$ (125.7 F/g) and $Ti_3C_2S_2$ (288.0 F/g) because Ti atoms in $Ti_3C_2$ accommodated the most charge transfer. This indicates that the properties of MXenes are generally hampered by the introduction of terminations. The −O and −S terminations on the surface affect the density of states near the Fermi level, resulting in degraded capacitance.

## 4. Manipulation of terminations: Surface modification and doping for energy storage applications

MXenes possess high theoretical capacity, good electrical conductivity, low working potential, fast ion diffusion, and good mechanical properties, exhibiting excellent performance in electrochemical energy storage devices such as batteries and supercapacitors. Shortly after its discovery, the first MXene ($Ti_2CT_x$) was experimentally determined to possess a capacity of 225 mAh/g at C/25 in Li-ion batteries [87]. Moreover, the MXene $Ti_3C_2T_x$was

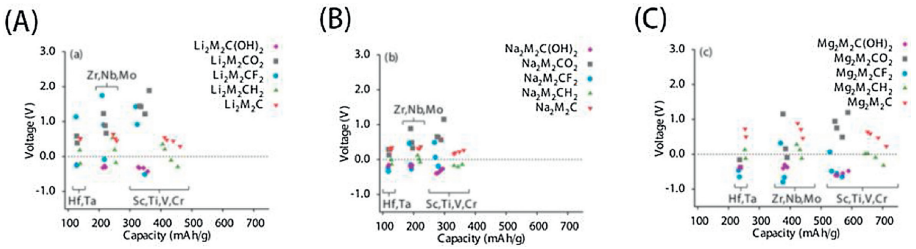


**Fig. 5.** Cell voltage and gravimetric capacity for intercalation of two ions per formula unit into $M_2CT_x$ phases containing various surface terminations. (A) $Li^+$ intercalation, (B) $Na^+$ intercalation and (C) $Mg^{2+}$ intercalation. Reproduced with permission [21]. Copyright 2014, American Chemical Society.

applied in supercapacitors with a volumetric capacitance of over 300 F/cm$^3$ at a scan rate of 2 mV/s [88]. The applications of MXenes in the energy storage field are increasing annually. Although the effect of MXene composition on its performance has not yet been systematically investigated, this does not prevent researchers from improving the performance of MXenes by tailoring their components. Because the terminations are extremely sensitive to the environment, many studies on surface modification and element doping have been performed to manipulate the terminations of MXenes, particularly in battery and supercapacitorapplications. Herein, we summarize strategies to improve the performance of MXenes by manipulating the terminations, as shown in Table 3. Despite the variable strategies, it should be noted that the performances of these materials are far below their theoretical values. This may be attributed to the complex composition of the surface terminations of the experimentally prepared MXenes.

### 4.1. Metal-ion batteries

Numerous studies have shown that a variety of metal ions, including $Li^+$, $Na^+$, $K^+$, $Al^{3+}$ and $Zn^{2+}$ as well as hydrated cation ions, can spontaneously intercalate into the interlayer space of MXene nanoflakes owing to the electrostatic effect from electronegative terminations. This promotes MXenes as ideal materials for ion battery electrodes. However, MXene-based electrodes also face great challenges: (1) low practical capacity, which is still far from the theoretical capacity; (2) the collapse and restacking of the multilayer structure, which reduces the conductivity; and (3) poor thermal stability. Surface terminations substantially affect the electrochemical performance of MXenes when applied as electrode materials. Heterogeneous element doping is a feasible approach capable of regulating the elemental composition of MXenes, thereby effectively improving their performance.

During the solution etching process, the choice of etchants and the control of temperature greatly affect the composition of the terminations [42,89]. Therefore, it is significant to optimize the reaction conditions to obtain terminations that are beneficial to the energy storage performance. A previous study on the thermal stability of $Ti_3C_2T_x$ proved that –OH terminations could be transformed at high temperatures to –O terminations. Gentile *et al.* [37] systematically studied the effect of the experimental parameters on the properties and performance of $Ti_3C_2T_x$ electrodes during HF etching and thermal treatment processes. The $Ti_3C_2T_x$ obtained at a high HF concentration followed by a 300 °C thermal treatment was mainly covered by –O terminations and exhibited an excellent capacity of 110 mAh/g at 30 mA/g. Kong *et al.*

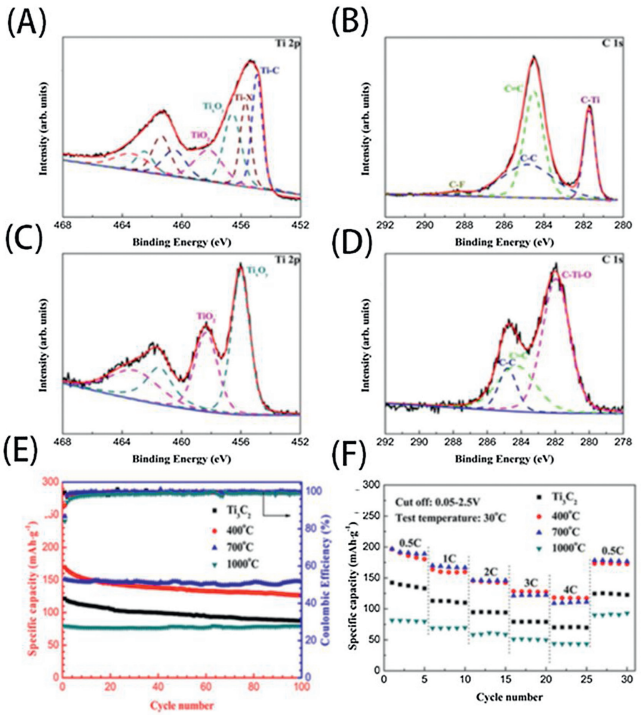


**Fig. 6.** High-resolution Ti 2p and C 1s XPS spectra of (A, B) initial $Ti_3C_2T_x$ and (C, D) $Ti_3C_2T_x$ calcined at 700 °C. (E) Cycling performance and Coulombic efficiency at 1 C. (F) Rate capacity at various rates (0.5, 1, 2, 3, 4 and 0.5 C). Reproduced with permission [90]. Copyright 2018, Elsevier.

[90] managed to remove part of the surface terminations on $Ti_3C_2T_x$ by heat treatment. As shown in Figs. 6A–D, the –OH and –F terminations partially transformed into –O terminations. Figs. 6E and F demonstrate that the $Ti_3C_2T_x$ treated at 400 °C showed a higher capacity (126.4 mAh/g at 1 C) compared with that of the initial $Ti_3C_2T_x$ (87.4 mAh/g). Lu *et al.* [91] demonstrated a convenient strategy to enhance Li-storage performance by annealing MXenes under hydrogen, which effectively removed –F terminations and transformed –OH terminations into –O ones. The obtained $Ti_3C_2T_x$ exhibited a lower interfacial charge transfer impedance and a higher volumetric specific capacity of ~123.7 mAh/cm$^3$. Similarly, Wang *et al.* [92] succeeded in replacing the surface –F termination with –O by treating $Ti_3C_2T_x$ at 300 °C in various atmospheres, and the Li-storage performance was significantly enhanced at low temperatures. A capacity of

**Table 3**
Termination manipulation in various energy storage devices.

| Applications | Strategies | Materials | Change in terminations [ref.] |
|---|---|---|---|
| Li-ion batteries | Vacuum calcination | $Ti_3C_2T_x$ | –OH and –F partially removed [90] |
| | Thermal treatment in air | $Ti_3C_2T_x$ | –O substituted –F [92] |
| | Annealing in hydrogen | $Ti_3C_2T_x$ | –F removed and –OH turned into –O [91] |
| | LiF/HCl etching | $Ti_2CT_x$ | –Cl appeared [42] |
| | Hydrothermal | N–$Nb_2CT_x$ | –N appeared [98] |
| Na-ion batteries | High HF concentration and thermal treatment | $Ti_3C_2T_x$ | less –F and more –O [37] |
| | Heating with thiourea in argon | S–$Ti_3C_2T_x$ | –S appeared [97] |
| | Shaking in KOH | Alkalized-$Ti_3C_2T_x$ | –OH substituted –F [89] |
| K-ion batteries | Shaking in KOH | Alkalized-$Ti_3C_2T_x$ | –OH substituted –F [89] |
| Li–S batteries | Hydrothermal | N–$Ti_3C_2T_x$/S | –N appeared [100] |
| Supercapacitors | $K^+$ intercalation and heat treatment in argon | KOH–$Ti_3C_2T_x$ | –OH and –F removed [106] |
| | Annealing under ammonia | N–$Ti_3C_2T_x$ | –F removed and –N appeared [109] |
| | Annealing under ammonia | N–$V_4C_3T_x$ | –N appeared [110] |
| | HCl and $NH_4F$ etching and annealing | N–$Ti_3C_2T_x$ | –N appeared [111] |
| | Hydrothermal with urea | N–$Ti_3C_2T_x$ | –N appeared [112] |
| | Urea intercalation and annealing in nitrogen | N-$Ti_3C_2T_x$ | –N appeared [113] |
| | Hydrothermal | NS-$Ti_3C_2T_x$ | –N and –S appeared [114] |

226 mAh/g (the 10th cycle) was observed at −20 °C, which was better than that of Cu–Zn alloys (below 200 mAh/g) [93], and a high capacity of 405 mAh/g was observed at room temperature (the 10th cycle).

In 2016, Kajiyama *et al.* [94] found that the interlayer distance of $Ti_3C_2T_x$ expanded with the intercalation of $Na^+$ ions, which led to improved cycling stability and a faster ion diffusion rate. In a further study, the relationship between the electrochemical performance and interlayer spacing of $Ti_2CT_x$ with different terminations was discussed [42]. $Ti_2CT_x$ obtained by the LiF/HCl etching method was found to be mainly terminated by −Cl, which expanded the interlayer spacing and endowed the electrode with a high energy density. However, this explanation is not fully convincing because the interlayer spacing can also be expanded by the intercalation of $Li^+$ ions. The authors also suggested that −Br and −I terminations could further expand the interlayer distance, thereby leading to substantially improved Li-ion accessibility. Luo *et al.* [95] raised an explanation named the "pillar effect," in which MXenes with larger interlayer spacings exhibit better electrochemical performance. In 2019, they intercalated S atoms into the interlayer of $Ti_3C_2T_x$ and formed Ti–S bonds [96]. The introduction of S terminations endowed the MXene with a large interlayerspacing for ion storage. Meanwhile, the electrodes showed a $Na^+$ storage capacity of 550 mAh/g at 0.1 A/g.

Heterogeneous element doping is a feasible approach for modifying the surface terminations of MXenes [97,98]. It is generally believed that heteroatoms are doped into the MXene structure by surface absorption and termination substitution. Li *et al.* [97] successfully introduced sulfur dopants into $Ti_3C_2T_x$ MXenes by hydrothermal treatment, which is briefly illustrated in Fig. 7A. The presence of a new Ti–S $2p_{3/2}$ peak in the X-ray photoelectron spectroscopy (XPS) spectrum in Fig. 7C compared with that in Fig. 7B confirms that the doped S atoms existed as surface terminations. The obtained S–$Ti_3C_2T_x$ exhibited a high reversible capacity of 183.2 mAh/g at 0.1 A/g as well as good rate capacities of 121.3 mAh/g at 2 A/g and 113.9 mAh/g at 4 A/g when applied as the anode materials in Na-ion batteries, as shown in Figs. 7D and E. These improvements are mainly attributed to the increased interlayer spacing and enhanced conductivity.

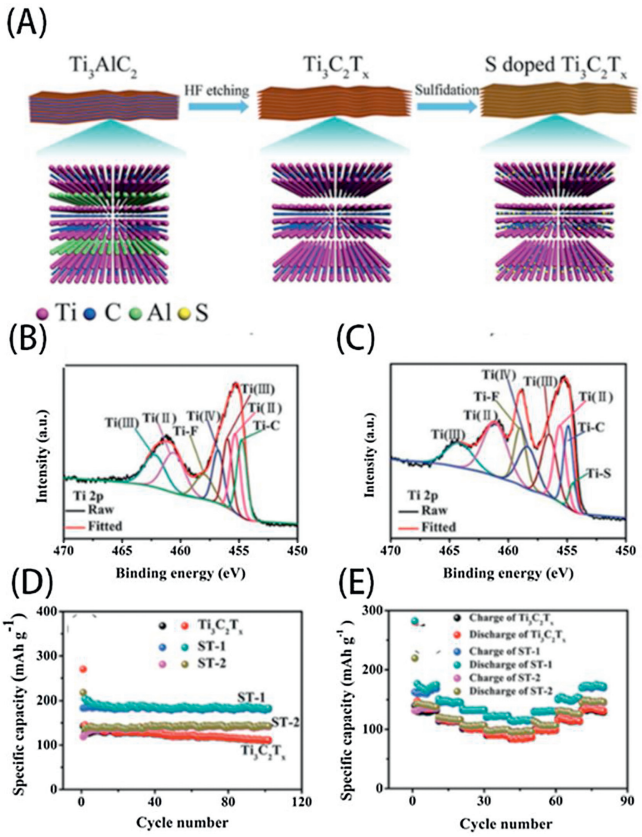


**Fig. 7.** (A) Schematic of the preparation of S-doped $Ti_3C_2T_x$. High-resolution Ti 2p spectra of (B) $Ti_3C_2T_x$ and (C) S-doped $Ti_3C_2T_x$. (D) Cycling performance and Coulombic efficiency at 0.1 A/g. (E) Rate performances. Reproduced with permission [97]. Copyright 2013, Royal Society of Chemistry.

### 4.2. Metal–sulfur batteries

Metal–sulfur batteries are considered to be the next-generation secondary batteries because of their high energy density and extensive sources of sulfur, among which lithium–sulfur batteries are the most widely studied. However, their practical application is still hampered by poor cycling stability, fast capacity decay caused by the large volume change inthe sulfur positive electrode, and the shuttle effect of polysulfides during charging/discharging. A general approach to overcome the above issues is to load sulfur on conductive materials with porous structures, such as carbon. After this successful discovery, MXenes are considered to be ideal sulfur host materials, which not only satisfy the conductivity requirement but also suppress the shuttle effect of polysulfides by forming strong chemical absorption. In 2015, Liang *et al.* [99] first prepared $Ti_2CT_x$/S as a cathode material for lithium–sulfur batteries. Since then, the application of MXenes in metal–sulfur batteries has become an active area of research. Unfortunately, most studies focus on the construction of MXene-based composite materials, while few reports are available at present that emphasize the interaction between terminations and polysulfides.

Theoretical simulation results imply that the absorption of polysulfides on MXenes is strongly dependent on the surface terminationspecies. Rao *et al.* [100] calculated the binding energies of $Li_2S_m$ on $Ti_2C(OH)_2$, $Ti_2CO_2$ and $Ti_2CF_2$ using density function theory (DFT). The attraction of $Ti_2C(OH)_2$ for $Li_2S_m$ was considerably stronger than that from $Ti_2CO_2$ and $Ti_2CF_2$, which induced the distortion of the $Li_2S_m$ lattice on $Ti_2C(OH)_2$. Liu *et al.* [101] proposed that the sulfur-terminated $Ti_2C$ MXene ($Ti_2CS_2$) possessed a higher efficiency in suppressing the shuttle effect than those of $Ti_2CO_2$ and $Ti_2CF_2$, originating from the higher affinity for polysulfides.

Bao *et al.* [102] synthesized nitrogen-doped $Ti_3C_2T_x$ MXene nanosheets with a crumple morphology through the thermal annealing of electronegative MXenes with electropositive melamine, as shown in Fig. 8A. From the XPS results in Figs. 8B–D, the doped N atoms were confirmed to exist as surface terminations. The N-doped $Ti_3C_2T_x$/S cathodes exhibited excellent electrochemical performance: a high reversible capacity (1144 mAh/g at 0.2 C, where 1 C = 1675 mA/g) and good cycling stability (610 mAh/g at 2 C after 1000 cycles), as shown in Figs. 8E and F. The excellent cycling performance was attributed to the effective inhibition of the shuttle effect. The doped nitrogen atoms increased the surface polarity and thus significantly enhanced the absorption effects of N–$Ti_3C_2T_x$ nanosheets on polysulfides, according to the ultraviolet/visible adsorption experiments.

### 4.3. Supercapacitors

The good mechanical properties, excellent electrical conductivity, excellent hydrophilicity, and high specific surface area of MXenes make them applicable as electrode materials for supercapacitors. Moreover, the existence of some hydrophilic terminations endows MXenes with excellent wettability and accessibility to the electrolyte. The influence of the electrolyte on the capacitive behavior of MXenes has been widely reported;

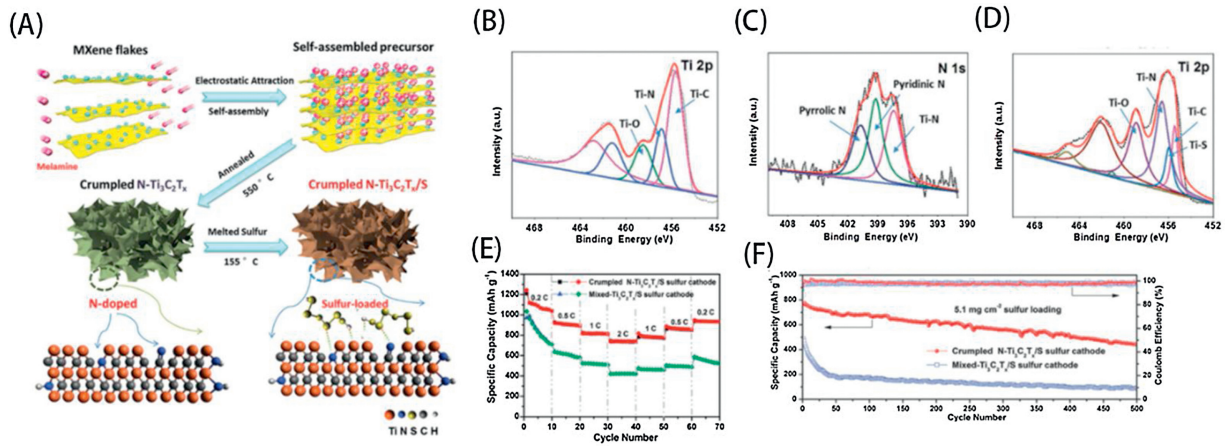


**Fig. 8.** (A) Schematic of the synthesis of crumpled N–$Ti_3C_2T_x$/S composites. (B) Ti 2p XPS spectrum of crumpled N–$Ti_3C_2T_x$ nanosheets. (C) N 1s spectrum of crumpled N–$Ti_3C_2T_x$ nanosheets. (D) Ti 2p spectrum of crumpled N–$Ti_3C_2T_x$/S composites. (E) Rate performances. (F) Cycling performance. Reproduced with permission [102]. Copyright 2018, Elsevier.

when applied in acidic electrolytes, $H^+$ ions can redox with –O terminations on the surface, which improves the capacitance by contributing to the pseudocapacitance and results in the cyclic voltammetry (CV) curves appear as twisted rectangles. Hu *et al.* [103] analyzed the *in situ* Raman spectroscopy characterization of $Ti_3C_2T_x$ during the electrochemical process in $(NH_4)_2SO_4$, $MgSO_4$ and $H_2SO_4$ electrolytes. It was demonstrated that hydronium in $H_2SO_4$ bonded with the –O terminations on the surface upon discharging and debonded upon charging, resulting in pseudocapacitance. Similar conclusions were reported by Lukatskaya *et al.* [104] according to X-ray absorption spectroscopy characterization, as follows:

$$Ti_3C_2O_x(OH)_yF_{2-x-y} + \delta H^+ + \delta e^- = Ti_3C_2O_{x-\delta}(OH)_{y+\delta}F_{2-x-y} \quad (9)$$

Apart from contributing to the capacitance, surface terminations also affect many other aspects of the electrochemical properties of electrodes. For instance, –F terminations hinder the transfer of electrolyte ions and reduce the specific gravity of Ti atoms [105]. Because the Ti–F bond is less stable at higher pH, alkali treatment is considered a feasible strategy to replace –F with –OH. In 2017, Li *et al.* [106] removed most of the –F terminations from $Ti_3C_2T_x$ through KOH alkalization and heat treatment to obtain a substantial enhancement in the gravimetric capacitance (517 F/g at a charging rate of 1 A/g), which is approximately twice as large as that of the original $Ti_3C_2T_x$. Similarly, Zhang *et al.* [107] prepared a $Ti_3C_2T_x$ MXene, followed by alkalinizing and annealing treatments. The obtained $Ti_3C_2T_x$ film exhibited an ultrahigh volumetric capacitance (1805 F/cm$^3$ at 1 A/g) and impressive cycling stability (up to 98% capacitance retention after 8000 cycles).

Heteroatomic doping, particularly nitrogen doping, has been widely studied in MXenes [108–114]. Lu *et al.* [108] systematically studied the atomic positions and effects of nitrogen dopants in MXenes. DFT simulations revealed that N dopants were most likely to substitute for –OH terminations among the three sites, with a formation energy of –4.71 eV. This replacement caused a change in the interlayer spacing and surface absorptions, which improved the electrical double-layer capacitance (EDLC) and

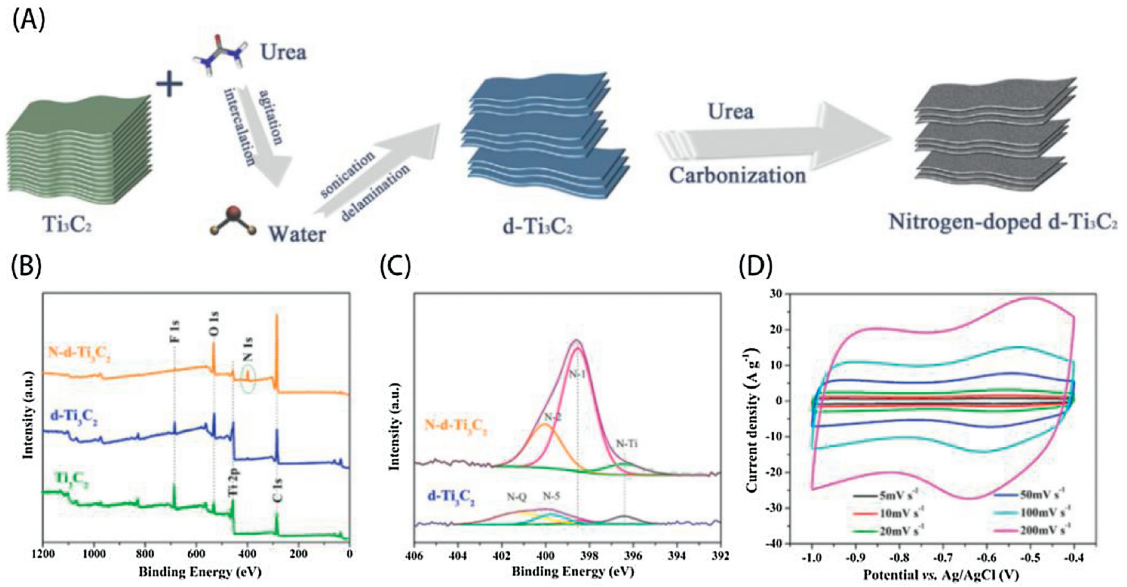


**Fig. 9.** (A) Schematic of the synthesis process of nitrogen-doped delaminated $Ti_3C_2T_x$ nanosheets. (B) XPS survey spectra of the $Ti_3C_2T_x$, D-$Ti_3C_2T_x$ and N-D-$Ti_3C_2T_x$ samples. (C) High-resolution XPS spectra of the deconvolved N 1s peaks of the D-$Ti_3C_2T_x$ and N-D-$Ti_3C_2T_x$ samples. (D) CV curves of N-D-$Ti_3C_2T_x$ at different scan rates. Reproduced with permission [113]. Copyright 2017, Elsevier.

pseudocapacitance. In 2017, Wen *et al.* [109] achieved N-doped $Ti_3C_2T_x$ electrodes by annealing in an ammonia atmosphere. Heat treatment not only decreased the concentration of –F termination on the surface but also intercalated nitrogen atoms into the lattice, which expanded the interlayer spacing. The N-doped $Ti_3C_2T_x$ MXenes exhibited excellent electrochemical capacitances of 192 F/g in a 1 mol/L $H_2SO_4$ electrolyte and 82 F/g in a 1 mol/L $MgSO_4$ electrolyte. Tian *et al.* [111] synthesized N-modified $Ti_3C_2T_x$ using HCl and $NH_4F$ etching, followed by annealing. Afterward, the film heated at 300 °C exhibited good electrochemical performance. It had a gravimetric capacitance of 415.0 F/g at 2 mV/s in a 3 mol/L $H_2SO_4$ aqueous electrolyte, in which the –N terminations contributed by providing intercalation pseudocapacitance. Yang *et al.* [113] prepared nitrogen-doped $Ti_3C_2T_x$ using the scheme shown in Fig. 9A. The XPS survey spectra in Figs. 9B and C demonstrate that –N terminations were introduced while the number of –F terminations were diminished. These materials exhibited a high specific capacitance in a KOH electrolyte solution, as shown in Fig. 9D. They also reported nitrogen and sulfur co-doped $Ti_3C_2T_x$ as a high-capacity electrode [114]. The doping of N and S enhanced the intercalation of ions in the electrolyte and provided abundant electrical charge. The obtained nanosheets exhibited a high specific capacitance of 175 F/g at 2 mV/s in a 1 mol/L $Li_2SO_4$ electrolyte solution and excellent cycling stability (90.1% of the initial value after 5000 cycles).

## 5. Conclusion and prospects

As a new group of two-dimensional materials, MXenes have attracted tremendous attention in the energy storage field, even though it has been less than 10 years since the first report. In this review, we summarized studies on the terminations of MXenes, which include the origination, properties, and performance in energy storage fields.

The choice of etchants in the synthesis of MXenes has a strong impact on the composition of the surface terminations. MXenes obtained by fluorine-based etching methods are generally covered by hydrophilic terminations, including –OH, –O and –F. Alkali and electrochemically assisted etching methods yield non-F-terminated MXenes but demonstrate a much lower efficiency. Molten salt etching results in MXenes with nearly single terminations, which can be replaced through substitution reactions.

The electrochemical properties of MXenes are influenced by the composition of the surface terminations, which affects the adsorption and diffusion behaviors of metal ions on the surface. Furthermore, the interlayer spacing depends on the atomic size of the surface terminations. Among the available terminations in the literature, –O, –S and –N are predicted to favor the energy storage performance of MXenes, while –OH and –F are not. Heat treatment and heteroatom doping are effective methods for altering MXene surface terminations. By removing inferior terminations and introducing superior ones, the performance of MXenes in energy storage devices can be substantially improved.

With the discovery of an increasing number of approaches to obtain MXenes, the regulation of MXenes has gradually become an active area of research. Based on current research results, we believe the following aspects are important research directions for MXene terminations in the near future.

(1) Because terminations are inevitable, it is of great importance to find new conducive terminations that can improve the electrochemical performance of MXenes.
(2) Although many theoretical calculations and simulations have been reported to predict the influence of terminations on MXene properties and performance, sophisticated experimental designs are required to verify these theoretical predictions.
(3) The evolution of terminations during electrochemical ion storage is currently not clear. Therefore, advanced characterization technologies, particularly operando technologies, are required.
(4) New synthesis methodologies are highly desired to accurately control the species of terminations. In addition, post-processing, such as annealing and alkali treatment, has a strong influence on the species of terminations, which deserves great attention in the future.

## Declaration of competing interest

The authors report no declarations of interest.

## Acknowledgments

This research was funded by the National Natural Science Foundation of China (Nos. 51731004 and 51902051) and Natural Science Foundation of Jiangsu Province (No. BK20200386). The authors would also like to thank all members of the research group for discussion and advice.

## References

[1] S.Z. Butler, S.M. Hollen, L.Y. Cao, et al., ACS Nano 7 (2013) 2898–2926.
[2] M.S. Xu, T. Liang, M.M. Shi, et al., Chem. Rev. 113 (2013) 3766–3798.
[3] M. Chhowalla, H.S. Shin, G. Eda, et al., Nat. Chem. 5 (2013) 263–275.
[4] H. Zhang, ACS Nano 9 (2015) 9451–9469.
[5] K.S. Novoselov, A.K. Geim, S.V. Morozov, et al., Science 306 (2004) 666–669.
[6] D. Golberg, Y. Bando, Y. Huang, et al., ACS Nano 4 (2010) 2979–2993.
[7] Q.H. Wang, K. Kalantar-Zadeh, A. Kis, et al., Nat. Nanotechnol. 7 (2012) 699–712.
[8] P. Vogt, P. De Padova, C. Quaresima, et al., Phys. Rev. Lett. 108 (2012) 155501.
[9] E. Bianco, S. Butler, S.S. Jiang, et al., ACS Nano 7 (2013) 4414–4421.
[10] H.O. Churchill, P. Jarillo-Herrero, Nat. Nanotechnol. 9 (2014) 330–331.
[11] M. Naguib, M. Kurtoglu, V. Presser, et al., Adv. Mater. 23 (2011) 4248–4253.
[12] Babak Anasori, Y. Gogotsi, 2D Metal Carbides and Nitrides (MXenes), Springer, Cham, 2019.
[13] O. Mashtalir, M. Naguib, B. Dyatkin, et al., Mater. Chem. Phys. 139 (2013) 147–152.
[14] M.A. Hope, A.C. Forse, K.J. Griffith, et al., Phys. Chem. Chem. Phys. 18 (2016) 5099–5102.
[15] T. Hu, J. Wang, H. Zhang, et al., Phys. Chem. Chem. Phys. 17 (2015) 9997–10003.
[16] G.R. Berdiyorov, AIP Adv. 6 (2016) 055105.
[17] Q. Tang, Z. Zhou, P. Shen, J. Am. Chem. Soc. 134 (2012) 16909–16916.
[18] S. Lai, J. Jeon, S.K. Jang, et al., Nanoscale 7 (2015) 19390–19396.
[19] C. Si, J. Zhou, Z. Sun, ACS Appl. Mater. Interfaces 7 (2015) 17510–17515.
[20] C. Si, K.H. Jin, J. Zhou, et al., Nano Lett. 16 (2016) 6584–6591.
[21] C. Eames, M.S. Islam, J. Am. Chem. Soc. 136 (2014) 16270–16276.
[22] I. Persson, A. El Ghazaly, Q. Tao, et al., Small 14 (2018) 1703676.
[23] J. Halim, J. Palisaitis, J. Lu, et al., ACS Appl. Nano Mater. 1 (2018) 2455–2460.
[24] R. Meshkian, M. Dahlqvist, J. Lu, et al., Adv. Mater. 30 (2018) 1706409.
[25] M. Naguib, O. Mashtalir, J. Carle, et al., ACS Nano 6 (2012) 1322–1331.
[26] M. Naguib, J. Halim, J. Lu, et al., J. Am. Chem. Soc. 135 (2013) 15966–15969.
[27] J. Halim, S. Kota, M.R. Lukatskaya, et al., Adv. Funct. Mater. 26 (2016) 3118–3127.
[28] B. Anasori, Y. Xie, M. Beidaghi, et al., ACS Nano 9 (2015) 9507–9516.
[29] R. Meshkian, Q. Tao, M. Dahlqvist, et al., Acta Mater. 125 (2017) 476–480.
[30] J. Zhou, X. Zha, F.Y. Chen, et al., Angew. Chem. Int. Ed. 55 (2016) 5008–5013.
[31] J. Zhou, X. Zha, X. Zhou, et al., ACS Nano 11 (2017) 3841–3850.
[32] M.H. Tran, T. Schäfer, A. Shahraei, et al., ACS Appl. Energ. Mater. 1 (2018) 3908–3914.
[33] M. Ghidiu, M. Naguib, C. Shi, et al., Chem. Commun. (Camb.) 50 (2014) 9517–9520.
[34] J. Yang, M. Naguib, M. Ghidiu, et al., J. Am. Ceram. Soc. 99 (2016) 660–666.
[35] X. Zhang, Z. Zhang, Z. Zhou, J. Energy Chem. 27 (2018) 73–85.
[36] M. Alhabeb, K. Maleski, T.S. Mathis, et al., Angew. Chem. Int. Ed. 57 (2018) 5444–5448.
[37] A. Gentile, C. Ferrara, S. Tosoni, et al., Small Methods 4 (2020) 2000314.
[38] J. Luo, W. Zhang, H. Yuan, et al., ACS Nano 11 (2017) 2459–2469.
[39] M. Ghidiu, M.R. Lukatskaya, M.Q. Zhao, et al., Nature 516 (2014) 78–81.
[40] A. Lipatov, M. Alhabeb, M.R. Lukatskaya, et al., Adv. Electron. Mater. 2 (2016) 1600255.
[41] F. Liu, A. Zhou, J. Chen, et al., Appl. Surf. Sci. 416 (2017) 781–789.
[42] S. Kajiyama, L. Szabova, H. Iinuma, et al., Adv. Energy Mater. 7 (2017) 1601873.
[43] Z. Li, L. Wang, D. Sun, et al., Mater. Sci. Eng. B 191 (2015) 33–40.

[44] G. Ying, A.D. Dillon, A.T. Fafarman, et al., Mater. Res. Lett. 5 (2017) 391–398.
[45] F. Liu, J. Zhou, S. Wang, et al., J. Electrochem. Soc. 164 (2017) A709–A713.
[46] S. Yazdanparast, S. Soltanmohammad, A. Fash-White, et al., ACS Appl. Mater. Interfaces 12 (2020) 20129–20137.
[47] B. Soundiraraju, B.K. George, ACS Nano 11 (2017) 8892–8900.
[48] X. Li, J. Hao, R. Liu, et al., Energy Storage Mater. 33 (2020) 62–70.
[49] F. Li, Y.L. Liu, G.G. Wang, et al., J. Mater. Chem. A: Mater. Energy Sustain. 7 (2019) 22631–22641.
[50] C. Cui, R. Cheng, H. Zhang, et al., Adv. Funct. Mater. 30 (2020) 2000693.
[51] Q. Guo, X. Zhang, F. Zhao, et al., ACS Nano 14 (2020) 2788–2797.
[52] J. Halim, M.R. Lukatskaya, K.M. Cook, et al., Chem. Mater. 26 (2014) 2374–2381.
[53] A. Feng, Y. Yu, F. Jiang, et al., Ceram. Int. 43 (2017) 6322–6328.
[54] V. Natu, R. Pai, M. Sokol, et al., Chem 6 (2020) 616–630.
[55] P. Urbankowski, B. Anasori, T. Makaryan, et al., Nanoscale 8 (2016) 11385–11391.
[56] M. Li, J. Lu, K. Luo, et al., J. Am. Chem. Soc. 141 (2019) 4730–4737.
[57] Y. Li, H. Shao, Z. Lin, et al., Nat. Mater. 19 (2020) 894–899.
[58] V. Kamysbayev, A.S. Filatov, H. Hu, et al., Science 369 (2020) 979–983.
[59] G. Li, L. Tan, Y. Zhang, et al., Langmuir 33 (2017) 9000–9006.
[60] T. Li, L. Yao, Q. Liu, et al., Angew. Chem. Int. Ed. 57 (2018) 6115–6119.
[61] W. Sun, S.A. Shah, Y. Chen, et al., J. Mater. Chem. A: Mater. Energy Sustain. 5 (2017) 21663–21668.
[62] S. Yang, P. Zhang, F. Wang, et al., Angew. Chem. Int. Ed. 57 (2018) 15491–15495.
[63] S.Y. Pang, Y.T. Wong, S. Yuan, et al., J. Am. Chem. Soc. 141 (2019) 9610–9616.
[64] J. Mei, G.A. Ayoko, C. Hu, et al., Sustain. Mater. Technol. 25 (2020) e00156.
[65] J. Mei, G.A. Ayoko, C. Hu, et al., Chem. Eng. J. 395 (2020) 125111.
[66] X.H. Zha, K. Luo, Q. Li, et al., Europhys. Lett. 111 (2015) 26007.
[67] A.N. Enyashin, A.L. Ivanovskii, J. Phys. Chem. C 117 (2013) 13637–13643.
[68] A. Champagne, L. Shi, T. Ouisse, et al., Phys. Rev. B 97 (2018) 115439.
[69] M. Khazaei, M. Arai, T. Sasaki, et al., Adv. Funct. Mater. 23 (2013) 2185–2192.
[70] M. Khazaei, M. Arai, T. Sasaki, et al., Phys. Chem. Chem. Phys. 16 (2014) 7841–7849.
[71] M. Khazaei, A. Ranjbar, M. Arai, et al., J. Mater. Chem. C: Mater. Opt. Electron. Devices 5 (2017) 2488–2503.
[72] H. Weng, A. Ranjbar, Y. Liang, et al., Phys. Rev. B 92 (2015) 075436.
[73] M. Khazaei, A. Ranjbar, M. Ghorbani-Asl, et al., Phys. Rev. B 93 (2016) 205125.
[74] Y. Wang, M. Zhou, L.C. Xu, et al., J. Power Sources 451 (2020) 227791.
[75] Y. Wang, J. Shen, L.C. Xu, et al., Phys. Chem. Chem. Phys. 21 (2019) 18559–18568.
[76] J. Hu, B. Xu, C. Ouyang, et al., J. Phys. Chem. C 118 (2014) 24274–24281.
[77] B. Yan, C. Lu, P. Zhang, et al., Mater. Today Commun. 22 (2020) 100713.
[78] V. Mehta, H.S. Saini, S. Srivastava, et al., J. Phys. Chem. C 123 (2019) 25052–25060.
[79] V. Shukla, N.K. Jena, S.R. Naqvi, et al., Nano Energy 58 (2019) 877–885.
[80] S. Lee, S.C. Jung, Y.K. Han, Nanoscale 12 (2020) 5324–5331.
[81] N. Li, Y. Li, X. Zhu, et al., J. Phys. Chem. C 124 (2020) 14978–14986.
[82] Y. Xie, M. Naguib, V.N. Mochalin, et al., J. Am. Chem. Soc. 136 (2014) 6385–6394.
[83] Q. Meng, J. Ma, Y. Zhang, et al., Nanoscale 10 (2018) 3385–3392.
[84] X. Wang, S. Kajiyama, H. Iinuma, et al., Nat. Commun. 6 (2015) 6544.
[85] Y. Ando, M. Okubo, A. Yamada, et al., Adv. Funct. Mater. 30 (2020) 2000820.
[86] L. Wang, J. Wang, Z. Zhang, et al., J. Mater. Chem. A: Mater. Energy Sustain. 7 (2019) 16231–16238.
[87] M. Naguib, J. Come, B. Dyatkin, et al., Electrochem. commun. 16 (2012) 61–64.
[88] M.R. Lukatskaya, O. Mashtalir, C.E. Ren, et al., Science 341 (2013) 1502–1505.
[89] P. Lian, Y. Dong, Z.S. Wu, et al., Nano Energy 40 (2017) 1–8.
[90] F. Kong, X. He, Q. Liu, et al., Electrochim. Acta 265 (2018) 140–150.
[91] M. Lu, H. Li, W. Han, et al., J. Energy Chem. 31 (2019) 148–153.
[92] Y. Wang, C. Ma, W. Ma, et al., 2d Mater. 6 (2019) 045025.
[93] A. Varzi, L. Mattarozzi, S. Cattarin, et al., Adv. Energy Mater. 8 (2018) 1701706.
[94] S. Kajiyama, L. Szabova, K. Sodeyama, et al., ACS Nano 10 (2016) 3334–3341.
[95] J. Luo, X. Tao, J. Zhang, et al., ACS Nano 10 (2016) 2491–2499.
[96] J. Luo, J. Zheng, J. Nai, et al., Adv. Funct. Mater. 29 (2019) 1808107.
[97] J. Li, D. Yan, S. Hou, et al., J. Mater. Chem. A: Mater. Energy Sustain. 6 (2018) 1234–1243.
[98] R. Liu, W. Cao, D. Han, et al., J. Alloys. Compd. 793 (2019) 505–511.
[99] X. Liang, A. Garsuch, L.F. Nazar, Angew. Chem. Int. Ed. 54 (2015) 3907–3911.
[100] D. Rao, L. Zhang, Y. Wang, et al., J. Phys. Chem. C 121 (2017) 11047–11054.
[101] X. Liu, X. Shao, F. Li, et al., Appl. Surf. Sci. 455 (2018) 522–526.
[102] W. Bao, L. Liu, C. Wang, et al., Adv. Energy Mater. 8 (2018) 1702485.
[103] M. Hu, Z. Li, T. Hu, et al., ACS Nano 10 (2016) 11344–11350.
[104] M.R. Lukatskaya, S.M. Bak, X. Yu, et al., Adv. Energy Mater. 5 (2015) 1500589.
[105] X. Zang, J. Wang, Y. Qin, et al., Nano-Micro Lett. 12 (2020) 77.
[106] J. Li, X. Yuan, C. Lin, et al., Adv. Energy Mater. 7 (2017) 1602725.
[107] X. Zhang, Y. Liu, S. Dong, et al., Electrochim. Acta 294 (2019) 233–239.
[108] C. Lu, L. Yang, B. Yan, et al., Adv. Funct. Mater. 30 (2020) 2000852.
[109] Y. Wen, T.E. Rufford, X. Chen, et al., Nano Energy 38 (2017) 368–376.
[110] H. Li, X. Wang, H. Li, et al., J. Alloy. Compds. 784 (2019) 923–930.
[111] Y. Tian, W. Que, Y. Luo, et al., J. Mater. Chem. A: Mater. Energy Sustain. 7 (2019) 5416–5425.
[112] Y. Tang, J. Zhu, W. Wu, et al., J. Electrochem. Soc. 164 (2017) A923–A929.
[113] C. Yang, W. Que, X. Yin, et al., Electrochim. Acta 225 (2017) 416–424.
[114] C. Yang, W. Que, Y. Tang, et al., J. Electrochem. Soc. 164 (2017) A1939–A1945.